Free Radicals and Polymerization of Resinous Materials Used in Dentistry

6

Bruno Luiz Santana Vicentin and Eduardo Di Mauro

6.1 Introduction

A composite is generally defined as a material composed of two or more distinct phases. Dental composites consist of a polymerizable resin base containing a ceramic filler that does not interfere on the polymerization reaction. Most dental polymers are based on acrylic resins made up of monomethacrylate, dimethacrylate, or trimethacrylate monomers. The most common restorative materials are based on the bisphenol A-bis(glycidyl methacrylate) (Bis-GMA), which copolymerizes with triethylene glycol dimethacrylate (TEGDMA). Also the dimethacrylate monomers bisphenol A-dimethacrylate (Bis-EMA) and a urethane dimethacrylate (UDMA) are commonly used [1].

Photopolymerizable composite resins are the best substitutes for restoring the lost part of a tooth, both esthetically and practically, because a substitute with similar properties to the human tooth still does not exist. These composite resins polymerize by the absorption of blue visible light which activates the photoinitiator camphorquinone (CQ) from the ground state to an excited state where it reacts with a hydrogen donor and produces an initiating free radical (FR). Thus the excited molecule interacts with other molecules to form FRs capable of starting the radical polymerization by rapid addition of monomers to the chain [1, 2].

B. L. S. Vicentin (✉)
Department of Physics, State University of Londrina, Londrina, Brazil
e-mail: bruno.vicentin@uel.br

E. Di Mauro
Laboratório de Ressonância Paramagnética Eletrônica (LARPE), Departamento de Física – CCE, Universidade Estadual de Londrina, Londrina, Paraná, Brazil
e-mail: dimauro@uel.br

A. K. Shukla (ed.), *Electron Spin Resonance Spectroscopy in Medicine*,
https://doi.org/10.1007/978-981-13-2230-3_6

Besides composite resins used to restore the lost part of the tooth, acrylic resin cements are used to retain intraradicular post for the purpose of assisting the retention of the restoration material. In general, dental resin cements are dual cured to ensure polymerization at deepest points of the restoration where radiation cannot excite CQ, such that photo-cure and self-cure happen simultaneously and independently [1, 3]. Self-curing cements are two-component filled systems based on dimethacrylate monomers with an organic peroxide, usually benzoyl peroxide (BPO). To promote the decomposition of BPO at oral temperature, cold-cure acrylic resins need another chemical, usually an aromatic tertiary amine, to carry out the redox initiation, together with BPO in a short period of time [1, 3].

Intraradicular posts manufactured from a composite of glass fibers and epoxy resin are often used in the treatment of teeth for the purpose of assisting the retention of the restoration material. The fiberglass post became popular in dental practice because of its physical properties, which are very similar to dentin, for its adhesion to root dentin and its esthetic qualities, which differ considerably from the cast metal post. The retention of the fiberglass post with resin material directly depends on the degree of conversion of the cement selected. Thus, translucent fiberglass posts were developed for the purpose of transmitting light and improving cement polymerization throughout the length of the root canal. The efficiency of light transmission by the post, and hence the improvement in the degree of resin cement conversion, is directly proportional to the post diameter [4, 5].

However, these resins do not polymerize completely, and this causes problems that can compromise the restoration. Numerous factors affect polymerization, including chemical composition, polymerization conditions, light intensity, and distance from the device to the resin, which can compromise the restoration and cause problems, such as contraction, poor mechanical strength, color change, and infiltration. In order to avoid these problems and improve the mechanical properties of the restoration, a clearer understanding of the polymerization process is important.

A polymerization reaction encompasses three stages: initiation, propagation, and termination. In the initiation stage, the reaction is started by generating free radicals, and these radicals react with first monomer. In the propagation stage, successive reactions with monomers occur until the reaction is terminated, typically by combination of monomers or disproportionation. Consider R^* being a primary radical (generated by a redox reaction or blue visible light irradiation) and M the monomer molecule.

The general reaction mechanism for the free radical polymerization with termination by combination of monomer is as follows [1]:

Initiation:

$$R^* + M \xrightarrow{k_i} \mathrm{RM}_1^* \tag{6.1}$$

Propagation:

$$\mathrm{RM}_1^* + M \xrightarrow{k_p} \mathrm{RM}_2^* \tag{6.2}$$

$$\mathrm{RM}_2^* + M \xrightarrow{k_p} \mathrm{RM}_3^* \tag{6.3}$$

.
.
.

$$\mathrm{RM}_x^* + M \xrightarrow{k_p} \mathrm{RM}_{x+1}^* \tag{6.4}$$

Termination:

$$\mathrm{RM}_n^* + \mathrm{RM}_m^* \xrightarrow{k_t} \mathrm{RM}_{m+n}R \tag{6.5}$$

In these reactions, k_i, k_p, and k_t denote the reaction rate constants of the initiation, propagation, and termination stages, respectively.

Since these FRs generated are paramagnetic species, electron magnetic resonance (EMR) spectroscopy is a reliable technique for identifying and quantifying the concentration of FRs in the sample without any changes in the material composition. In this way, it is possible to identify the free radicals generated by each initiation mode either to resin composites or to resin cements. In addition, the degree of conversion of monomers into polymer is related to the amount of FRs generated during the initiation step of the polymerization reaction.

This chapter is divided into three parts: (1) multifrequency EMR for identification of radicals, (2) real-time polymerization monitoring by EMR, and (3) influence of the translucent fiberglass post on the depth of polymerization in a root canal.

6.2 Multifrequency EMR for Identification of Free Radicals

6.2.1 Free Radicals in a Photo-Cured Resin Composite

For more than 40 years, EMR spectroscopy has been used to detect, characterize, and monitor the evolution of free radical concentration in dental resins. This spectroscopic technique has been used to study the behavior of the methacrylate radical generated during photopolymerization of dental restoration resins in numerous situations, including irradiation at different wavelengths, required polymerization time as a function of resin composition or sample thickness, resin hardness as a function of the relative number of radicals, conversion degree, analysis of polymerization initiator agents, real-time study of polymerization kinetics, variations in the monomer matrix and influence on the chemical reaction, the effect of the saturation time, evaluation of the behavior of free radicals versus mechanical properties, the relation between the free radicals generated and polymerization depth in resin with different colors, and translucence. Some research has been conducted to elucidate the well-known, though not fully interpreted, nine-line EMR spectrum

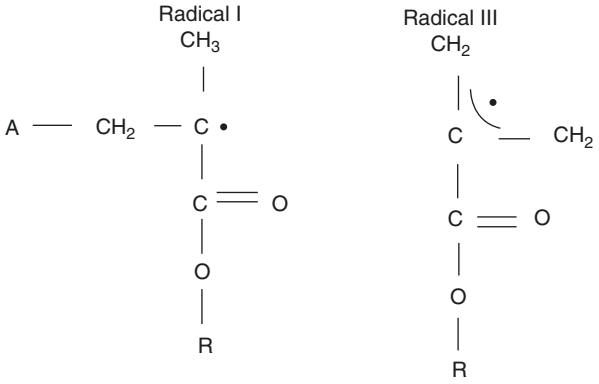

Fig. 6.1 Free radicals generated during the photopolymerization of dental resin Z100 (3 M ESPE) that are responsible for the EMR spectrum formation, where A is the amine monomer and R is dimethacrylate monomer mixture of Bis-GMA and TEGDMA

obtained in X-band for the radicals of methacrylate monomers. Some authors have attributed this spectrum to only one radical specimen. It is currently accepted that this spectrum is due to at least two different free radical types, which are assumed to occur simultaneously in the samples under study. Some authors assumed that the EMR spectrum is formed by the sum "5 + 4" lines; however, the intensities of the lines obtained using this model are different from those in the dental resin spectrum. Truffier-Boutry et al. [6] have assumed that the spectrum is generated from two methacrylate radicals in the solid state (Fig. 6.1), the "propagating" radical (RI) and the allylic radical (RIII). In addition, the methacrylate radical (RII) is probably not observed in the EMR spectrum because it reacts rapidly or the quantity generated is too small to detect, such that the resulting EMR spectrum is formed by the superposition of "9 + 5" lines.

Samples of the commercial resin Z100 (3 M ESPE, Campinas, SP, Brazil), in A2 color indicated for dental enamel, were used in the EMR experiments. It is composed essentially of a dimethacrylate monomer mixture of Bis-GMA and TEGDMA, initiator agents (camphorquinone and amine), and charge particles of zirconium and silica (ZrO_2/SiO_2) (manufacturer's specifications). The light source used for photopolymerization was a LED (Ultra Blue, Dabi Atlante, Ribeirão Preto, SP, Brazil) with an intensity 492 mW/cm^2 for 40 s.

The EMR spectra in X-band (~9 GHz) were obtained in a JEOL (JES-PE-3X) spectrometer at room temperature, and the microwave power (1 mW), modulation amplitude (0.40 mT), and modulation frequency (100 kHz) were set to avoid signal saturation and were maintained constant. A JEOL standard sample MgO:Mn^{2+} was used as intensity standard and g marker. The samples were placed in a 2 × 2 mm silicon mold and 40 s of irradiation [1–6]. The EMR spectra in Q-band were obtained with a VARIAN (E-109) spectrometer, with rectangular cavity, microwave power 0.5 mW, and modulation amplitude 0.40 mT. A MgO:Cr^{3+} was used as intensity standard and g marker, where g = 1.9797. The samples were placed in a 1 × 1 mm silicon mold and irradiated for 40 s. The EMR spectra in W-band were obtained in a Bruker (Elexsys E 680) spectrometer with TerraFlex probe, with sample dimensions of less than 1 mm. The data treatment was

performed with the Origin (OriginLab) software, and simulations were achieved using the WinEPR (Bruker) software.

The free radicals produce an EMR signal with hyperfine splitting, and the resulting spectrum shows an intense signal that remains detectable up to 3 months after the polymerization process began, depending on the storage environment and relative concentration generated.

The EMR spectrum was simulated based on the model proposed by Truffier-Boutry et al. [6]. Radical I is the "propagating" methacrylate radical (CH_2–C*–CH_3) that shows a weak nine-line signal, while the other simulated radical, RIII (CH_2–C*–CH_2), has a strong five-line signal arising from a stable radical, called an allylic radical (Fig. 6.1) [1].

The EMR spectrum of polymethacrylate radicals consists of the superposition of nine-line (RI) and five-line (RIII) sets resulting in a "nine-line spectrum" with peaks of alternating intensities, because the hyperfine interaction of the five-line set is about twofold greater than that of the nine-line set and the first line of both sets are virtually coincident (Fig. 6.2). Thus, the proposed model is a "9+5 line spectrum," and not a "5+4 line spectrum."

Regarding the spectrum simulation, Lorentzian and Gaussian shapes were both considered, with different proportions, because these two line shapes are commonly observed in EMR.

The spin Hamiltonian for radicals I and III can be represented as

$$H_{\mathrm{I}} = \mathrm{g}\beta\mathrm{HS} + \left[\mathrm{AIS} + \mathrm{BIS} + \mathrm{B}'\mathrm{IS}\right], \tag{6.6}$$

for radical I, and

$$H_{\mathrm{III}} = \mathrm{g}\beta\mathrm{HS} + \left[\mathrm{AIS} + \mathrm{BIS}\right], \tag{6.7}$$

for radical III, where gßHS is the Zeeman effect and AIS, BIS, and B′IS are the hyperfine interactions of first and second orders, respectively. The hyperfine structure with nine lines was interpreted and simulated in terms of an unpaired electron interaction, with three equivalent protons of the CH_3 group and two non-equivalent protons of the CH_2 group for radical I, and the interaction of radical III with two CH_2 groups, the radical generated during hydrogen abstraction of the monomer by an amine radical [1–3].

Figure 6.3a shows the EMR simulated spectrum for the radical I with this model, and Fig. 6.3b shows the simulated spectrum for radical III. The sum of these two spectrum gives the nine-line EMR spectrum shown in Fig. 6.3c, which is superimposed with the experiment.

In order to obtain additional information concerning the radicals that participate in the polymerization process, measurements were performed in other EMR bands, aimed at improving the spectrum resolution due to the use of higher frequencies. The same model was tested using the Q- and W-bands, due to their sensitivity, in order to detect other radical species; non-detection can occur when the radical is produced in very small amounts or in the case of species possessing very similar g

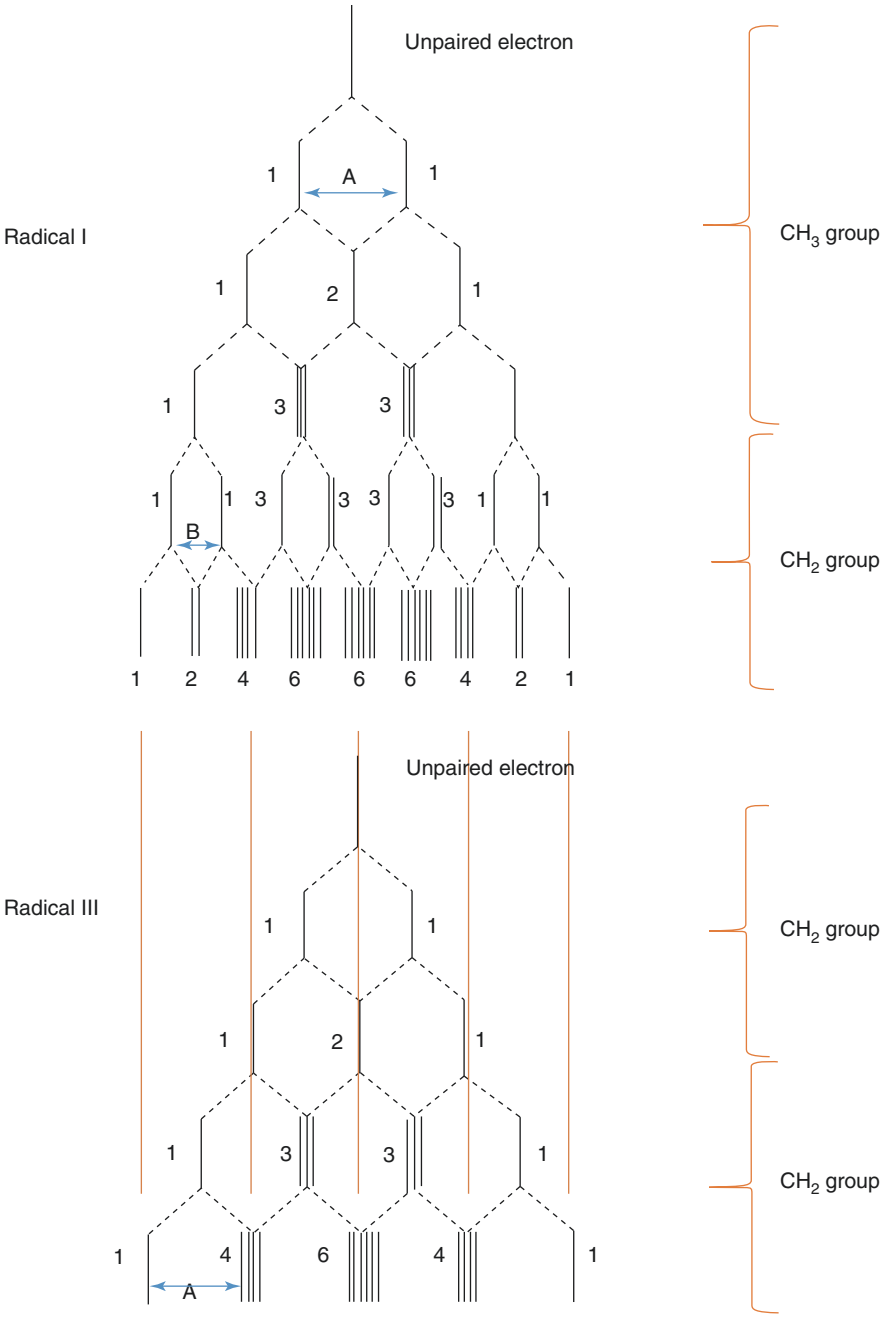

Fig. 6.2 Energy level diagram for the two radicals considered

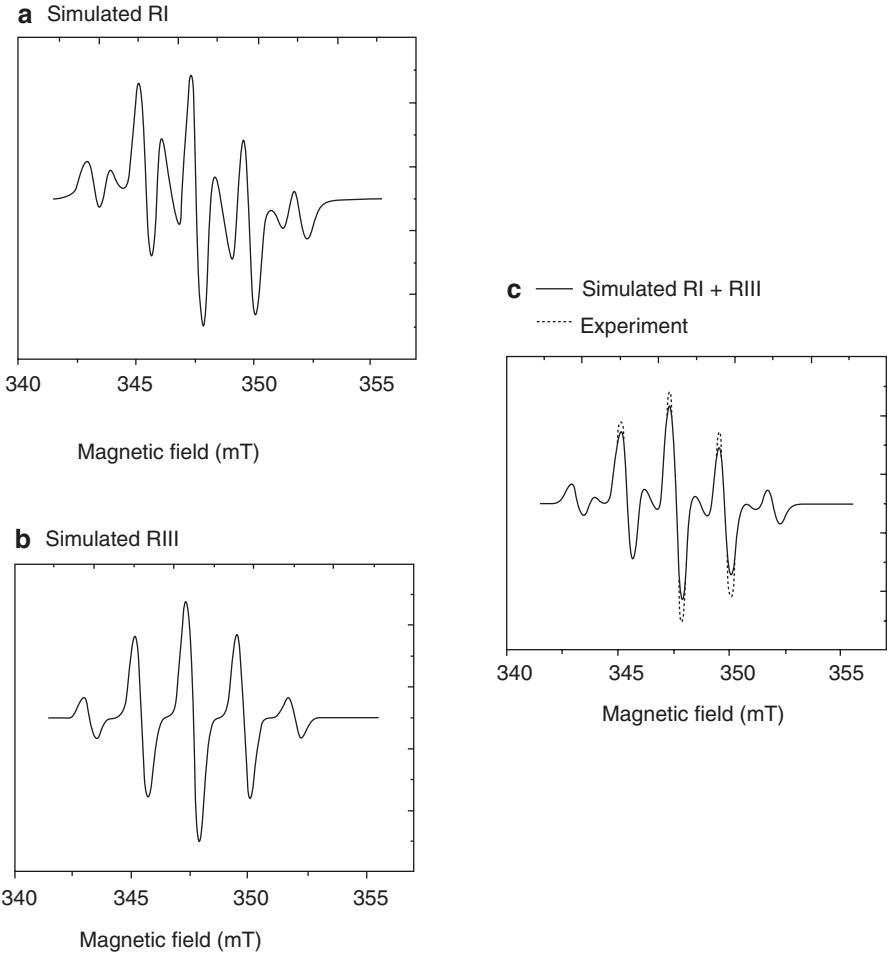

Fig. 6.3 Radical I (**a**) and radical III (**b**) EMR spectra simulations of the composite resin in X-band. (**c**) The superposition of simulated "RI + RIII" and experimental spectra

factors. Figure 6.4a, b shows the simulated spectra for radicals I and III in Q-band and Fig. 6.4c the superposition of simulated RI + RIII with experiment. Again the Hamiltonians and model proposed agree with experiment, as well as in W-band (Fig. 6.5). Since no changes in the spectrum formation were verified, the hypothesis of two radicals was considered valid [2].

The parameters obtained for the simulation in X-band for radical I, with $S = 1/2$ and $I = 1/2$, were $g = 2.0051$ and $A/g\beta = 2.17$ mT for three equivalent 1/2 spin protons belonging to the CH_3 group, $B/g\beta = 1.40$ mT for a non-equivalent proton belonging to the CH_2 group, and $B'/g\beta = 0.85$ mT for a second non-equivalent proton belonging to the CH_2 group. For radical III, the parameters used were $g = 2.0051$ and $A/g\beta = 2.17$ mT for two equivalent 1/2 spin protons belonging to the CH_2 group

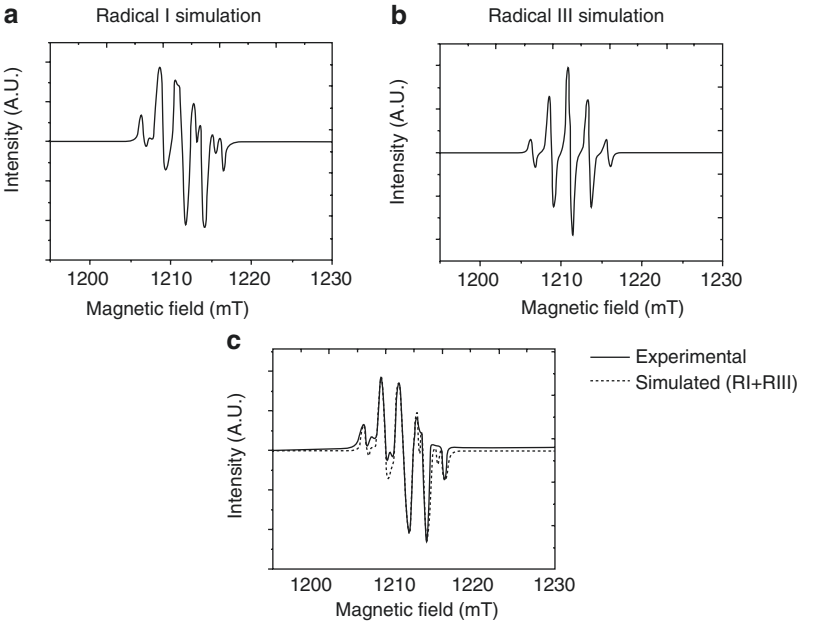

Fig. 6.4 Radical I (**a**) and radical III (**b**) EMR spectra simulations of the composite resin in Q-band. (**c**) Superposition of the simulated "RI + RIII" and experimental spectra

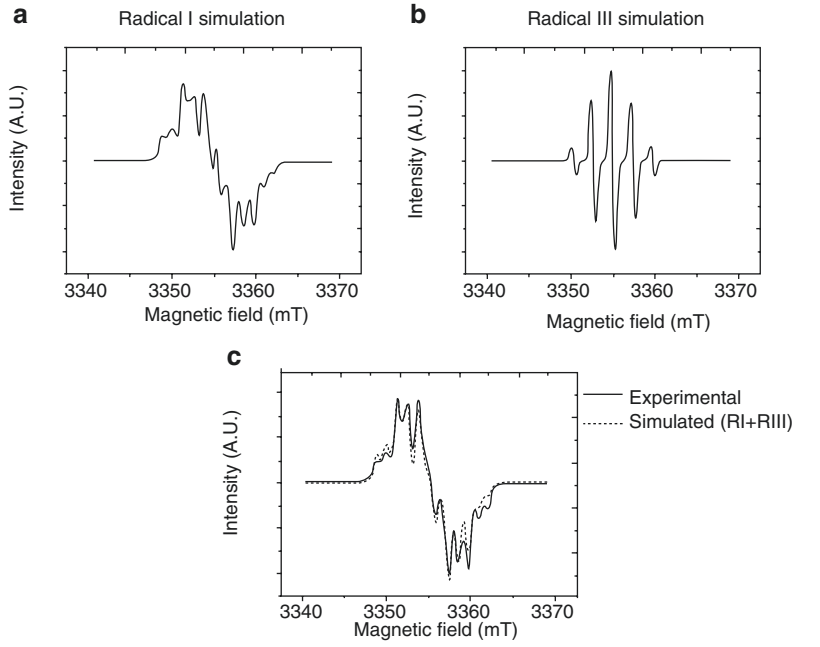

Fig. 6.5 EMR spectrum formation for the dental resin obtained in W-band. Radical I (**a**) and radical III (**b**), and the superposition of the experimental spectrum and the sum of the simulated spectra of radicals I and III (**c**)

and $B/g\beta$ = 2.17 mT for two equivalent 1/2 spin protons belonging to the second CH_2 group [2].

The parameters for the simulation in Q-band with 1/2 spin for radical I were $ACH_3x/g\beta$ = 2.32 mT, $ACH_3y/g\beta$ = 2.32 mT, and $ACH_3z/g\beta$ = 2.33 mT for three protons of the CH_3 group; $BCH_2x/g\beta$ = 1.30 mT, $BCH_2y/g\beta$ = 2.00 mT, and $BCH_2z/g\beta$ = 1.60 mT for one proton of the CH_2 group; $B'1CH_2x/g\beta$ = 0.95 mT, $B'1CH_2y/g\beta$ = 0.75 mT, and $B'1CH_2z/g\beta$ = 0.93 mT for 1 s proton of the CH_2 group; and gx = 2.0015, gy = 2.0023, gz = 2.0023, L/G = 0.5, lx = ly = 0.59 mT, and lz = 0.60 mT. For radical III, $ACH_2xyz/g\beta$ = 2.34 mT and $BCH_2xyz/g\beta$ = 2.34 mT are two CH_2 groups with four equivalent protons, $gxyz$ = 2.0020, lx = ly = 0.55 mT, and lz = 0.61 mT.

The parameters for the simulation in W-band with 1/2 spin for radical I were $ACH_3x/g\beta$ = 2.46 mT, $ACH_3y/g\beta$ = 2.48 mT, and $ACH_3z/g\beta$ = 2.50 mT for three protons of the CH_3 group; $BCH_2x/g\beta$ = 1.30 mT, $BCH_2y/g\beta$ = 1.40 mT, and $BCH_2z/g\beta$ = 1.45 mT for one proton of the CH_2 group; $B'1CH_2x/g\beta$ = 0.95 mT, $B'1CH_2y/g\beta$ = 0.97, and $B'1CH_2z/g\beta$ = 0.90 mT for 1 s proton of the CH_2 group; and gx = 2.00069, gy = 2.0028, gz = 2.0023, L/G = 0.5, lx = ly = 0.59 mT, and lz = 0.65 mT. For radical III, $ACH_2xyz/g\beta$ = 2.34 mT and $BCH_2xyz/g\beta$ = 2.34 mT are two CH_2 groups with four equivalent protons, $gxyz$ = 2.0020, lx = ly = 0.55 mT, and lz = 0.61 mT.

Analysis of the figures revealed that improvement in the EMR spectrum resolution is observed when a higher microwave frequency is used, due to the fact that the free radicals present in the resin are submitted to a more intense magnetic field, which permits the observation of a larger portion of the resonance lines of each radical. The majority the transitions observed in W-band occur in the region of superposed energy levels, hindering clearer identification of the same in X- and Q-bands. The advantage of measuring at higher frequencies is the improved resolution, which should assist in differentiating the paramagnetic species.

In relation to some little differences between experiments and simulations, it is important to remember that we simulate considering the macromolecular system with the unpaired electron interacting only with the closer vicinity, and the Hamiltonian is an approximation for this system in vacuum or water environment. The proper polymerization of the sample can also influence in the result. Considering the number of peaks, line shape, and other parameters, the simulations are in good agreement with experiment [2].

6.2.2 Free Radicals in a Dual-Cured Resin Cement

Samples of resins were dual-cured with cement from AllCem (FGM, Joinville, Brazil) in the color shade A1 were examined by X-, Q-, and W-band EMR. The initial compounds are two pastes separated in a dual-body syringe which are mixed in a self-mixing nozzle that accompanies the kit. The polymerization reaction begins upon mixing the base paste with the catalyst in the nozzle, and it can be accelerated by blue light irradiation. In all experiments, the initial paste and catalyst were mixed

in a 1:1 weight ratio. The particular resin cement was chosen for this study because it has the same composition and showed similar properties and quality compared to others used worldwide for the purpose of translucent fiberglass post cementation. The irradiation of the cement with the blue visible light was produced by a LED (Ultra Blue, Dabi Atlante, Ribeirão Preto, Brazil) with a potency of 492 mW/cm^2. The resin cement samples were separated into two major groups: irradiated for 40 s and not irradiated. Multifrequency EMR spectroscopy aims at improving the spectroscopic information from the use of different field strengths [3].

The X-band (~9 GHz) EMR spectra were obtained with a JEOL JES-PE-3X spectrometer at room temperature using 1 mW microwave power, 0.40 mT modulation amplitude, and 100 kHZ modulation frequency to avoid signal saturation. The samples were placed in a 2 × 2 mm Teflon mold. The Q-band EMR spectra were obtained with a Bruker ER-5106 QT spectrometer at 0.5 mW microwave power and 0.40 mT modulation amplitude. The samples were placed in a 1 × 1 mm Teflon mold. The W-band EMR spectra were obtained with a Bruker Elexsys E 680 spectrometer fitted with a TerraFlex probe, with sample dimensions of less than 1 mm. All experiments were carried out at room temperature. The data treatment was performed with OriginLab software, and simulations were achieved using the WinEPR (Bruker) software [3].

In addition to the self-cure, the dual-cure resin cement has the photo-cure initiators added to its composition. The photoinitiation mechanism by the camphorquinone reaction with a tertiary amine is well described by Truffier-Boutry et al. [6] for the composite resin and was analyzed in previous section. As the EMR spectrum does not depend on the inorganic charges and the self-cure takes place independently of the photo-cure, the model proposed by Truffier-Boutry et al. [6] is applicable to this case, such that the free radicals responsible for the continuity of the polymerization initiated by photo-cure are the propagating (CH_3–C*–CH_2) and the allylic (CH_2–C*–CH_2) radicals.

In the self-cure process, the BPO is degraded releasing two primary radicals and an inert product [3]. Figure 6.6 represents the BPO degradation by interaction with the tertiary amine 4(*N*,*N*-dimethylamino)phenethyl alcohol (DMPOH) [3]. The primary free radicals generated in the self-cure are the N-methylene radical (named PRI) and the benzoyloxy radical (named PRII), while the inert product is benzoic acid [3]. Subsequently PRI and PRII react with monomers leading to the induction step and then to the propagation step, where the active monomer reacts with another monomer molecules. The PRI reacts with monomers by breaking the double bonding or by hydrogen abstraction (Figs. 6.7 and 6.8). The reaction

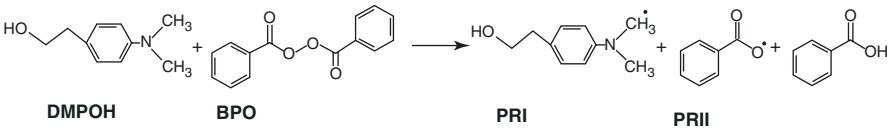

Fig. 6.6 The degradation process of BPO generating two primary radicals, PRI (N-methylene radical) and PRII (benzoyloxy radical), and one inert product

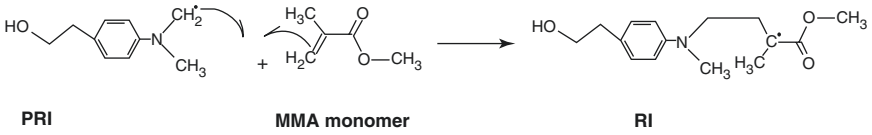

Fig. 6.7 The reaction of PRI with a MMA monomer generating the propagating radical (RI)

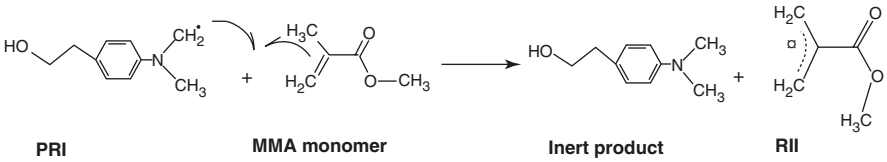

Fig. 6.8 Reaction of PRI with a MMA monomer by hydrogen abstraction generating an inert product and an allylic radical (RII)

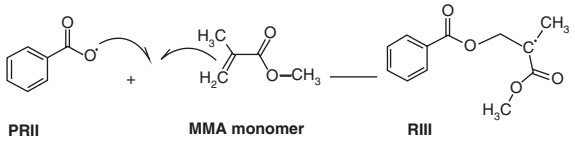

Fig. 6.9 The reaction of PRII with a MMA monomer generating the propagating radical (RIII)

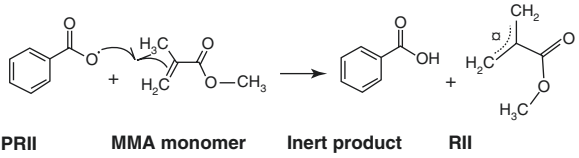

Fig. 6.10 Reaction of PRII with a MMA monomer by hydrogen abstraction generating an inert product and an allylic radical (RII)

generates two different radicals, the propagating radical (RI) and the allylic radical (RII), which can be detected by EMR spectroscopy. Figures 6.9 and 6.10 represent the reaction of the PRII with methacrylate monomer generating two different radicals, RIII and RII.

For mobile radicals, the radical structures RI, RII, and RIII are assumed. It is possible to see that the unpaired electrons in RI and RIII have the same neighborhood (CH_3–C*–CH_2), while RII has the CH_2–C*–CH_2 structure for the closest neighbors. These radicals are the same as the free radicals discussed by Truffier-Boutry et al. [6] to be responsible for the photopolymerization of a composite resin.

6.2.2.1 Multifrequency EMR Experiment

As the polymerization reaction occurs independent of each initiation protocol and the closest neighbors of the unpaired electrons are the same as those found in the composite resin shown by Fontes et al. [2], it is to be expected that the X-band EMR spectrum of the resin cement has nine lines. Figures 6.11 and 6.12a, b show the X-, Q-, and W-band EMR spectra, respectively, of the photo-cured and the self-cured sample.

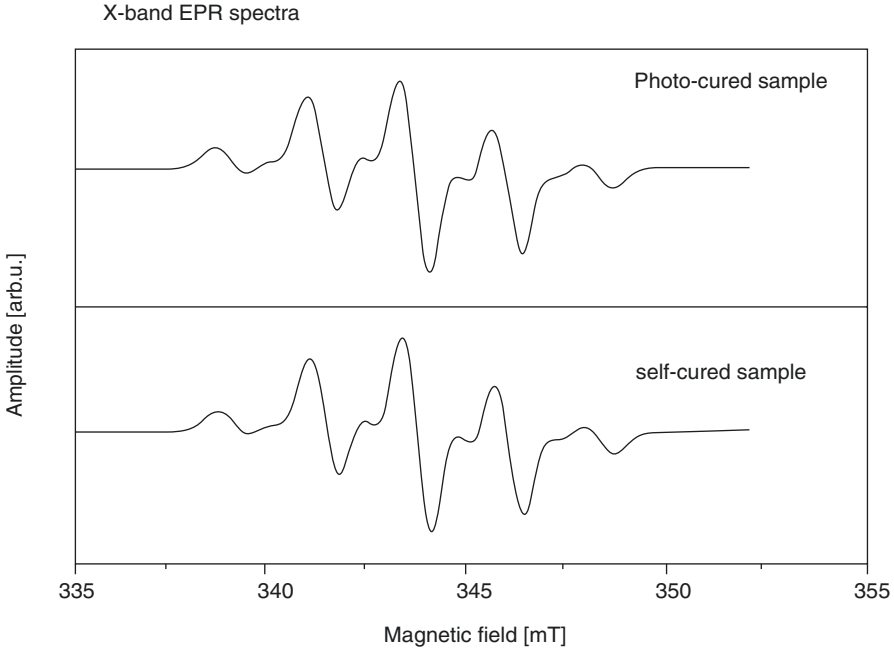

Fig. 6.11 X-band EPR spectra for the photo-cured and the self-cured samples of the dual-cure resin cement AllCem

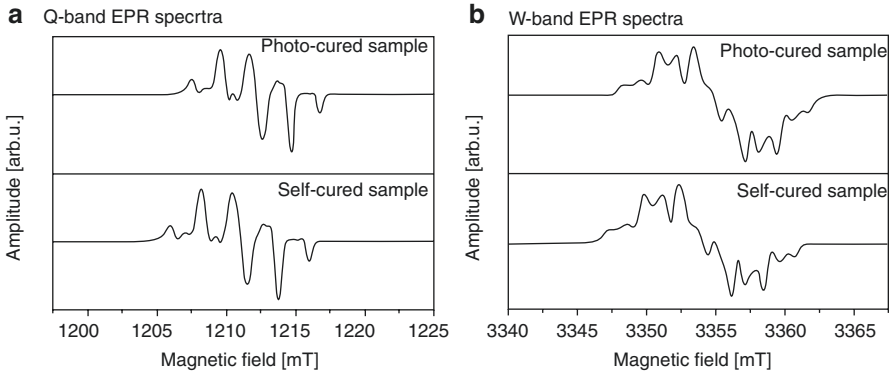

Fig. 6.12 EPR spectra for the photo-cured and the self-cured samples of the dual-cure resin cement AllCem in (**a**) Q-band and (**b**) W-band

No significant differences between photo-cure and self-cure are noticed, and the spectra agrees with the one obtained in previous section for the photopolymerizable dental resin. It is possible to conclude that for the dual-cured resin cement, there are two paramagnetic species forming the EMR spectrum, RI (CH_3–C*–CH_2) and RII (CH_2–C*–CH_2), which are the same radical species formed in the polymerization of the photo-cured composite resin. The radical species are simultaneously present in the sample and occur independently of the polymerization protocol [3].

6.3 Real-Time Polymerization Monitoring in Dental Composite by EMR

In this section, we demonstrate how electron magnetic resonance can be associated with nuclear magnetic resonance (NMR) to study the kinetics of polymerization. Again, the material chosen for the study is the commercial dual-cure resin cement AllCem (FGM).

The NMR-MOUSE (nuclear magnetic resonance mobile universal surface explorer) is a stray-field NMR device suitable to detect the monomer concentration and changes in molecular mobility nondestructively in real time [1]. The NMR-MOUSE can be used to acquire depth profiles locally into the object by varying the distance between the NMR-MOUSE and the object [1].

The concentration of FRs was determined by X-band EMR spectroscopy in real time during the reaction and correlated with the decay curve of mobile monomers obtained by the nuclear magnetic resonance mobile universal surface explorer (NMR-MOUSE). As the EPR signal intensity is proportional to the amount of paramagnetic species in the sample, the second integral of the spectrum gives the number of FRs at the time of measurement. This is a reliable method for determining the amount of radical species in any sample. The EPR experiment does not give information about layers and positions in the sample as does the NMR-MOUSE. The EPR spectrum is always correspondent to the overall mass of the sample inside the resonant cavity [1].

Therefore, while by the time-resolved NMR we can accompany the conversion of monomers into polymers during the reaction, we can probe by EMR the concentration of FRs responsible for the polymerization in the same period [1].

6.3.1 Kinetics of Polymerization of the Self-Cure

Table 6.1 presents the reaction mechanisms for the self-cure.

Table 6.1 Reaction mechanism for the self-polymerization

Initiation:
First step: $A + I \xrightarrow{k_d} A^* + I^* + \text{inert product}$
Second step: $\begin{cases} I^* + M \xrightarrow{k_{i1}} \text{RM}_1^* \\ A^* + M \xrightarrow{k_{i2}} \text{RM}_1^* \end{cases}$
Propagation: $\text{RM}_n^* + M \xrightarrow{k_p} \text{RM}_{n+1}^*$
Termination by combination or disproportionation**: $\text{RM}_n^* + \text{RM}_m^* \xrightarrow{k_t} D_{n+m} \,/\, D_n + D_m$
Radical trapping: $\text{RM}_n^* \xrightarrow{k_b} \text{RM}_{n,b}^*$
Primary radical termination: $\begin{cases} I^* + \text{RM}_n^* \xrightarrow{k_{tp}} D_n \\ A^* + \text{RM}_n^* \xrightarrow{k_{tp}} D_n \end{cases}$
Chain transfer to amine: $\text{RM}_n^* + A \xrightarrow{k_{fA}} D_n + A^*$
Inhibition: $P_n^* + \text{ZA} \xrightarrow{k_Z} D_n$
Benzoyl peroxide side reaction: $I^* + I \xrightarrow{k_I} I^* + \text{inert product}$

**In these equations $n \approx m$

Based on the general kinetics mechanism presented for the self-cure of resin cement, rate equations for all the reacting species can be written as follows [1]:

Initiators:

$$\frac{\mathrm{d}[I]}{\mathrm{d}t} = k_d [I][A] + k_I [I^*][I] \tag{6.8}$$

$$-\frac{\mathrm{d}[A]}{\mathrm{d}t} = k_d [I][A] + k_{fA} [\text{RM}^*][I] \tag{6.9}$$

Primary initiator radicals:

$$-\frac{\mathrm{d}[I^*]}{\mathrm{d}t} = -f_1 k_d [I][A] + k_{i1} [I^*][M] + k_{tp} [I^*][\text{RM}^*] \tag{6.10}$$

$$-\frac{\mathrm{d}[A^*]}{\mathrm{d}t} = -f_2 k_d [I][A] + k_{i2} [A^*][M] + k_{tp} [A^*][\text{RM}^*] + k_{fA} [\text{RM}^*][A] \tag{6.11}$$

Double bonds:

$$-\frac{\mathrm{d}[M]}{\mathrm{d}t} = k_p [\text{RM}^*][M] + k_{i1} [I^*][M] + k_{i2} [A^*][M] \tag{6.12}$$

Active macroradicals:

$$-\frac{\mathrm{d}\left[\mathrm{RM}^{*}\right]}{\mathrm{d}t}=-k_{i1}\left[M\right]\left[I^{*}\right]-k_{i2}\left[M\right]\left[A^{*}\right]+2k_{t}\left[\mathrm{RM}^{*}\right]^{2}+k_{Z}\left[Z\right]\left[\mathrm{RM}^{*}\right]$$
$$+k_{b}\left[\mathrm{RM}^{*}\right]+k_{fA}\left[A\right]\left[\mathrm{RM}^{*}\right]+k_{tp}\left(\left[I^{*}\right]+\left[A^{*}\right]\right)\left[\mathrm{RM}^{*}\right] \tag{6.13}$$

Trapped radicals:

$$\frac{\mathrm{d}\left[\mathrm{RM}^{*}\right]_{b}}{\mathrm{d}t}=k_{b}\left[\mathrm{RM}^{*}\right] \tag{6.14}$$

Inhibitor:

$$\frac{\mathrm{d}\left[Z\right]}{\mathrm{d}t}=-k_{Z}\left[Z\right]\left[\mathrm{RM}^{*}\right] \tag{6.15}$$

In these equations $\left[\mathrm{RM}^{*}\right]=\sum_{n=1}^{\infty}\mathrm{RM}_{n}^{*}$ and k_b is the radical trapping rate constant, which is assumed to be dependent on the fractional free volume of the mixture (V_f) according to $k_\mathrm{b}=k_{\mathrm{b0}}\frac{1}{\mathrm{e}^{-\gamma_\mathrm{b}/V_\mathrm{f}}}$, with k_{b0} the pre-exponential factor, and γ_b is the dimensionless activation volume which governs the rate at which radical trapping increases as a function of fractional free volume. This set of differential ordinary equations can be numerically integrated with the Gear's method to give the time dependence of all reacting species.

During the initial stage of polymerization, where the effect of diffusion-controlled phenomena on the reaction rates is negligible and the steady-state approximation for macroradicals holds, the rate of polymerization (R_p) is given by [1]

$$R_{p}=k_{p}\left(k_{d}\frac{\left(f_{1}+f_{2}\right)}{k_{t}}\right)^{1/2}\left[M\right]\left(\left[I\right]\left[A\right]\right)^{1/2}. \tag{6.16}$$

where k_d is the initiator decomposition rate constant; k_p and k_t represent the propagation and termination rate constant, respectively; and f_1 and f_2 denote the efficiency factors.

6.3.2 Kinetics of Polymerization of the Photo-Cure

The initiator (I) is activated by light irradiation either to a singlet (lifetime in the nanosecond range) or a triplet state (with a lifetime of 50 ms) [1]. Triplet-activated CQ molecules $\left(I_{\mathrm{triplet}}^{*}\right)$ may react with the accelerator molecules (A) and fm two radicals [1], I^* and R^*. I^* shows little reactivity, and the polymerization rate is determined by accelerator radical R^* reacting with the first monomer M. In the propagation stage, the macromolecular chains are formed by successive reaction with monomers. The reaction is terminated typically by combination and/or disproportionation (Table 6.2) [1].

Table 6.2 Reaction mechanisms for the photo-cure

Initiation: $I + h\nu \rightarrow I^*_{\text{triplet}}$
$I^*_{\text{triplet}} + A \rightarrow I^* + R^*$
$R^* + \text{M} \xrightarrow{k_i} \text{RM}^*$
Propagation: $\text{RM}^*_n + \text{M}_1 \xrightarrow{k_p} \text{RM}^*_{n+1}$
Termination by combination or disproportionation**:
$\text{RM}^*_n + \text{RM}^*_m \xrightarrow{k_t} D_{m+n} \,/\, D_n + D_m$

**In these equations $n \approx m$

In these reactions, k_i, k_p, and k_t denote the reaction rate constant of the initiation, propagation, and termination steps, and D_{m+n} stands for the "dead" polymer formed containing $m + n$ monomer units.

The following classical analytical equations are developed for photo-cure kinetics for linear-chain systems [1]. If φ denotes the extinction coefficient assuming an infinite reservoir of accelerator molecules, I_0 the intensity of light absorbed in the surface, α the initiation efficiency, and d the length of the light path in the sample, the rate of production of primary radicals from the photo-sensitizer (R_{PR}) may be expressed by [1]

$$R_{PR} = k_i I_0 t \alpha \mathrm{e}^{-\varphi d}. \tag{6.17}$$

The rate of production of primary radicals can be re-expressed via the following equation:

$$R_{PR} = \beta k_i \left[A\right]\left[I^*_{\text{triplet}}\right], \tag{6.18}$$

where β is the fraction of exciplex "molecules" forming FR. Assuming that the rates of production and consumption of initiator radicals rapidly become equal (steady-state assumption), then R_{PR} is equal to the rate of initiation R_i, meaning $R_{PR} = R_i$ [1]. Approximating the rate of the bimolecular propagation reaction to be independent of the chain length, the propagation rate $R_p$may be expressed by

$$R_p = k_p \left[M\right]\left[\text{RM}^*\right], \tag{6.19}$$

where $[M]$ is the monomer concentration and $[\text{RM}^*]$ the concentration of growing chains. The reaction rate for termination by combination and/or disproportionation is written as

$$R_t = 2k_t \left[\text{RM}^*\right]^2 \tag{6.20}$$

In these reactions, k_i, k_a, k_p, and k_t denote the reaction rate constant of the initiation, rate constant of formation of exciplex from the bimolecular reaction between amine and CQ, and reaction rate of the propagation and termination steps. Assuming a steady state, initiation and termination reaction rates are identical ($R_i = R_t$). Then the steady-state propagation rate of radical polymerization is given by

$$-\frac{\mathrm{d}[M]}{\mathrm{d}t} = k_p \left(\frac{k_i I_0 \alpha e^{-\varphi d}}{2k_t} \right)^{1/2} \sqrt{t}[M]. \tag{6.21}$$

This leads to the time-dependent monomer concentration, $[M](t)$,

$$[M](t) = [M]_0 \, \mathrm{e}^{-\frac{2}{3}\left(\frac{t-t_0}{\tau_P}\right)^{3/2}}, \tag{6.22}$$

with the initial time t_0, $[M]_0$ the initial monomer concentration, and $\tau_P = \left[k_p \left(\frac{k_i I_0 \alpha e^{-\varphi d}}{2k_t} \right)^{1/2} \right]^{-\frac{2}{3}}$ the characteristic time constant for the photo-cure [1].

The self-cure reaction starts as soon as the two components are mixed. The paste-paste self-cure composite has a storage problem, as the BPO mixed with the dimethacrylate monomer is sensitive to heat decomposition. Therefore, inhibitors are added to suppress the polymerization of monomers and prevent premature polymerization. In the case of self-cure composites, inhibitors also provide clinical working time (referred to as the inhibition period, or more commonly, the induction period) to the professional for manipulating materials. When the two pastes of the composite are mixed, the radicals formed by the reaction of the BPO and amine are unable to react with the monomers due to the action of inhibitors and oxygen during the induction period. Thus, inhibitors produce an inert product and completely stop polymerization until the inhibitors are consumed, after which polymerization proceeds at the same rate as if the inhibitor was absent [1]. Meanwhile, the material can be light cured at any time during the chemical (self-)polymerization period. When the resin cement is irradiated, the production rate of primary radical is very high, so that the concentration of inhibitor decreases in a very short time, which explains the rapid decrease in amplitude of the NMR-MOUSE signal in Fig. 6.13a.

It was empirically obtained an expression for the changes in the mobile monomers concentration in the self-cure reaction. During the inhibition time, it is assumed the rate of production of FRs to be identical to the rate of consumption of radicals by the inhibitors, because according to Fig. 6.13, there are no changes in the concentration of mobile monomer during the first minutes. Thereafter, the monomer concentration decays in an exponential way. Considering the rate of self-polymerization in Eq. (6.16), we postulate this rate to be time-dependent [1]:

$$-\frac{\mathrm{d}[M]}{\mathrm{d}t} = \left(K_{\mathrm{SC}}\right) \sqrt[2]{t}[M], \tag{6.23}$$

in which $K_{\mathrm{SC}} = k_p \left(k_d \frac{(f_1 + f_2)}{k_t} \right)^{1/2} \left([I][A]\right)^{1/2}$. This expression can be integrated to give the time-dependent monomer concentration,

$$[M](t) = [M]_0 \, \mathrm{e}^{-\frac{2}{3}\left(\frac{t-t_0}{\tau_{\mathrm{SC}}}\right)^{3/2}}, \tag{6.24}$$

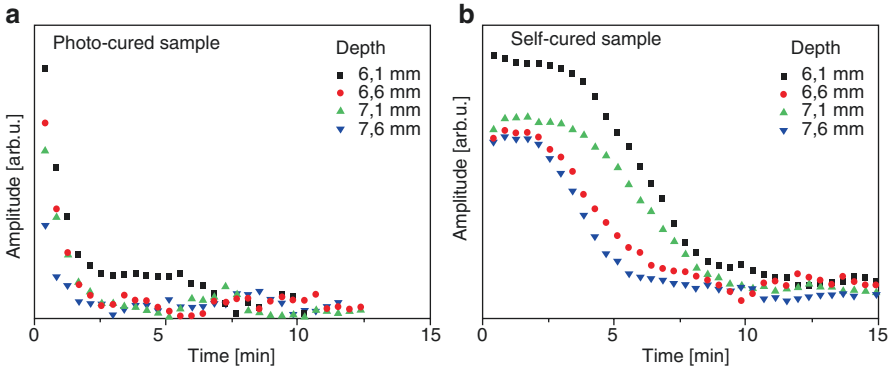

Fig. 6.13 Echo sums as function of time and depth corresponding to the distance to the sensor (**a**) for the photo-cured sample and (**b**) for the self-cured sample

with the initial time t_0 the average time for stopping the inhibition, $[M]_0$ the initial monomer concentration, and $\tau_{SC} = \left(K_{SC}\right)^{-2/3}$ the characteristic time constant of the self-cure reaction [1].

The entire curing process of a dual-cure resin without light irradiation is divided into three stages: the necessary working time for the dentistry professional, the conversion of monomers (curing time), and the cured sample (Fig. 6.14a). The EPR signal intensity for the self-cured sample first increases slowly during the time interval in which the monomers concentration is stable because of the presence of inhibitors to prevent premature reactions. In addition, oxygen trapped in the sample pans can act as an inhibitor [1]. Then the intensity rapidly decays once the concentration of inhibitors is zero. At this point the FRs can react with monomers and start the polymerization reaction. The EPR signal remains zero during the curing time of the resin cement because they are generated in the same rate that are consumed, as assumed in the solution for the rate equations. High initial initiator concentrations are used in commercial polymerizations in order to achieve fully cured products in short reaction times [1]. As the concentration of initiators is too large, FRs continue to be generated even after the monomers are converted into polymers (Fig. 6.14b), so the EPR signal intensity still grows after the curing time.

For the photo-cured sample, the amount of paramagnetic species detected in EPR spectroscopy grows up during the irradiation time and decreases after stopping irradiation (Fig. 6.15). The concentration of FRs rapidly increases up to a maximum value depending on the concentration of initiators, concentration of monomers, and other factors [1]. When irradiation is terminated, the concentration of FRs decreases exponentially due to the consumption of FRs when converting monomers to polymers [1]. The polymerization that occurs after irradiation is slow because the polymeric chain has low mobility in the matrix after irradiation. Figure 6.16 represents the proposed model.

The remaining FRs in a polymerized matrix have been widely studied [1]. During radical polymerization, a gel effect occurs [1], increasing the concentration of FRs which cannot terminate due to their reduced mobility in the matrix. In addition, a

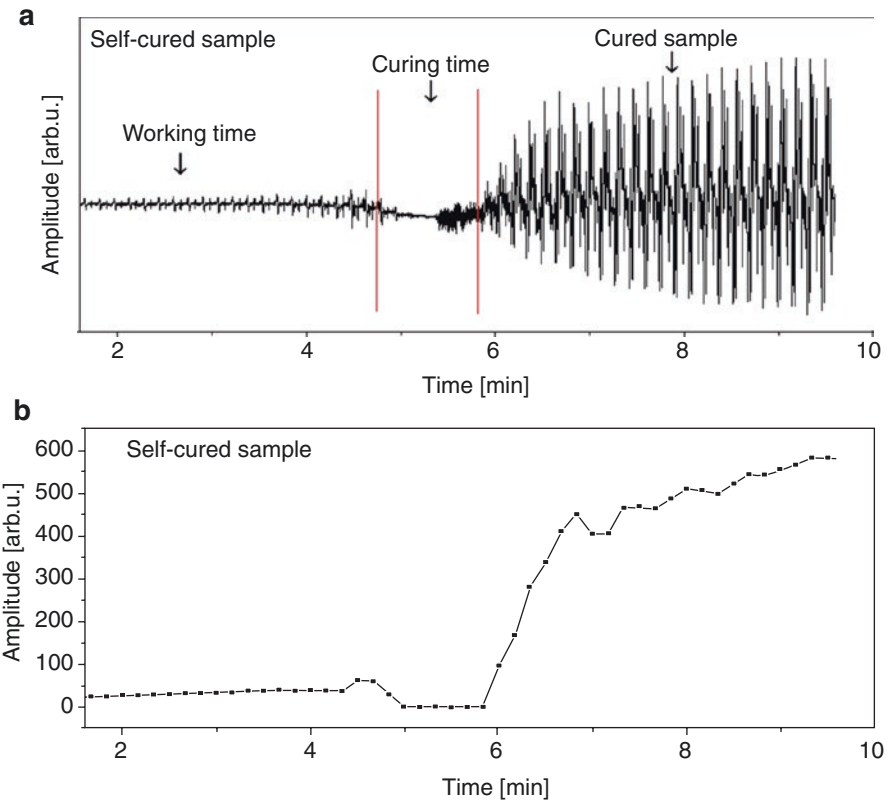

Fig. 6.14 (**a**) EPR spectra of the self-cured sample obtained every 10 s. (**b**) Intensity of the EPR spectra of the self-cured sample obtained every 10 s in a time interval of 10 min

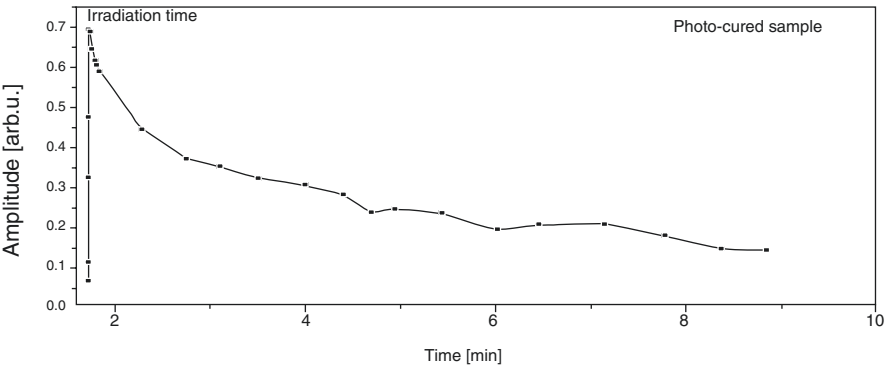

Fig. 6.15 Intensity of the EPR spectra of the photo-cured sample

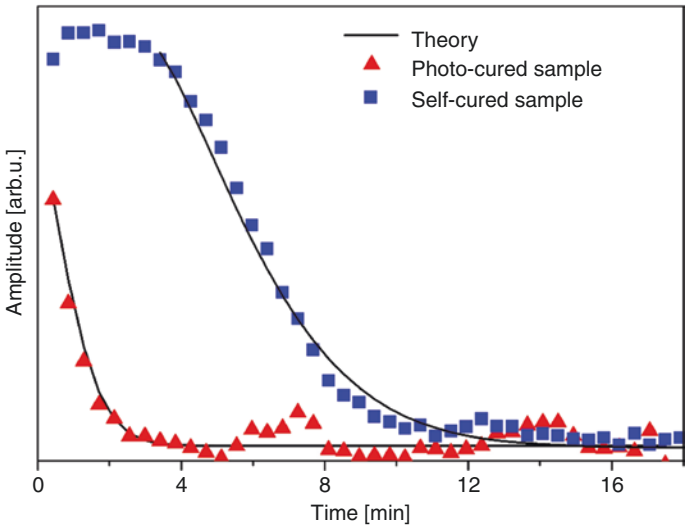

Fig. 6.16 Correlation between theory and experiment for the dual-cured resin cement

vitrification of the matrix occurs, and FRs and remaining double bonds are "quenched" in the organic matrix. Although FRs are present in the sample, the mobility of macromolecules is now in short range.

These results with real-time EPR spectroscopy can be related to the study with the NMR-MOUSE to confirm that the reduction in the concentration of mobile monomers traps FRs in the sample [1], and the model.

6.4 Influence of a Translucent Fiberglass Post on the Depth of Cure in a Root Canal

In this section, we show how EMR spectroscopy is a suitable tool to determine in an indirect way the degree of conversion of monomers into polymers. For this, we use a translucent fiberglass post cemented in a simulated root canal and measure the concentration of FRs in different depths of the post. As the degree of conversion directly depends on the concentration of free radicals generated during the initiation step, this study shows how the translucent fiberglass post effectively transmits the light from the curing device trough the root canal [6].

6.4.1 Influence of the Irradiation Mode and Depth of Cure in Double-Shaped Post

In this present experiment, the relative concentration of free radicals from the dual-cure resin cement, AllCem (FGM, Joinville, SC, Brazil; Table 6.1), of shade A1 was evaluated by electron paramagnetic resonance (EPR) at different restoration points,

after cementation of a prefabricated translucent fiberglass post White Post DC number 1 in a simulated root canal. These materials have properties and qualities that are very similar to others used worldwide. This methodology provides data and basement to understand the influence of a translucent fiberglass post on the degree of conversion of dual-cure resin cement.

The experiment is divided into three major groups: irradiated for 40 s (G1), not irradiated (G2), and irradiated for 40 s with the cementing line sealed (G3). In all groups, the post was cemented and then sectioned in three parts (cervical, middle, and apical thirds). By means of the relative concentration of free radicals, it is possible to study two variables: the influence of sealing the cementing line in the curing of the resin cement and the influence of the fiberglass post in the polymerization of resin cement at different depths (depth of cure of translucent fiberglass post).

After the post cementation for groups 1 and 3, the resin cement was photopolymerized for 40 s using a light-emitting diode (LED) (Radii Plus – SDI®, São Paulo, SP) with 1500 mW/cm^2 potency and in contact with the exposed fiberglass post (2 mm). In G3, the junction between the post and silicone interface was sealed prior to light curing to block light in this region. The resin cement was not photopolymerized after post cementation in G2.

After 10 min from the resin cement mixture, all specimens were removed from the silicone, and the 2 mm section of the fiberglass post that extended from the specimens was sectioned using a double-sided fine-grained diamond disc (Microdont, Socorro, SP, Brasil) at low speed. This sectioning left 18 mm of the post that was cemented, which was divided into three equal parts (6 mm each): the cervical third (closest to the silicon external surface), middle third, and apical third (furthest from the silicon external surface). A 2 mm sample from each third was obtained to study the relative concentration of free radicals: cervical third (CT), middle third (MT), and apical third (AT) (Fig. 6.17).

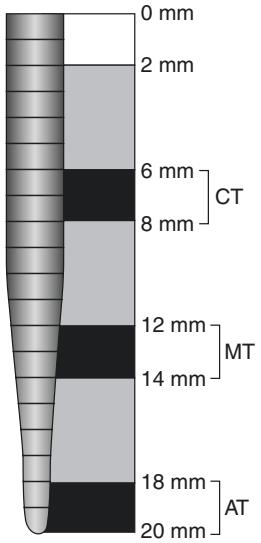

Fig. 6.17 Schematic representation of the double-shaped translucent fiberglass post and the thirds selected for the experiment

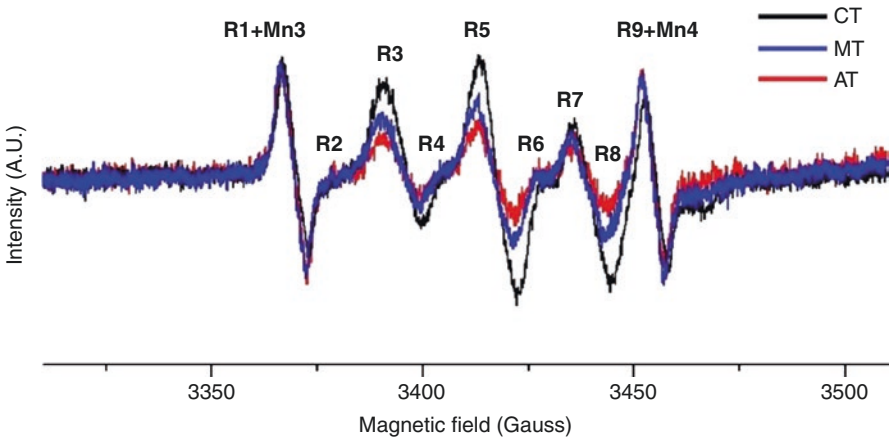

Fig. 6.18 The superposition of X-band EPR spectra for CT, MT, and AT of G1 with the manganese standard

Figure 6.18 shows the superposition of EPR spectra for CT, MT, and AT of G1 and illustrates how the comparison can be done. As CT showed the most intense EPR signal amplitude and thus the greatest concentration of free radicals for all experimental groups, it was taken as the reference point to study the variation on the relative concentration of free radicals between the samples in the group, so that the data presentation is relative to CT (taken as 100%) in each group. The first line in the EPR spectrum (Fig. 6.18) is the superposition of the third line of the MgO:Mn^{2+} standard (called Mn3) with the first line of the free radical (called R1), and the last line in the spectrum is the superposition of the fourth line of the standard (Mn_4) with the ninth line of the free radical (R9). The EPR signal intensity of free radicals for all groups was normalized with the line intensity of the third line of the MgO:Mn^{2+} standard to compare variances in the intensity of the free radical signal (central line) because the superposition is very small and does not change final intensity. As the replicates showed the same results, we used the samples with best signal to noise ratio for data treatment.

EPR spectra in X-band (~9 GHz) were obtained using a JEOL (JES-PE-3X) spectrometer at room temperature, and the microwave power (1 mW), modulation amplitude (20 Gauss), and modulation frequency (100 kHz) were set to avoid signal saturation. A JEOL standard sample MgO:Mn^{2+} was used as an intensity standard and g marker to determine the relative concentration of free radicals. The 2 mm samples from each third of fiberglass posts were inserted into quartz tubes with a 3 mm inner diameter and were analyzed 10 min (T0) and 24 h (T1) after cement mixing. In the time interval from T0 to T1, the samples were stored in aluminum envelopes to remove any influence of external radiation. The data obtained were processed using Origin 8 (OriginLab) and EasySpin (MatLab) software to process the EPR spectra. The estimated error in determining the intensity peak is ±6%.

The EPR spectrum in Fig. 6.18 shows nine-line characteristic of hyperfine interactions. It is concluded that the paramagnetic species in the sample are the "propagating" and "allylic" radicals shown by Fontes et al. [2], which generated during the irradiation of the sample. These radicals are present in the sample even 1 month after the irradiation because of the vitrification phenomenon, although in much less concentration. The reaction kinetics of dental materials is dependent on the initial concentration of monomers and initiators, as well as the light intensity and depth of cure and temperature. This supports the analysis in two different days and light intensity in this study.

6.4.1.1 The Influence of Irradiation Protocol

In relation to the amount of free radicals generated using different initiation methods, the present resin cement displayed a dependence of this quantity with the sample irradiation protocols (Table 6.3).

The chemical cure occurs regardless of the physical cure, a fact verified by the EPR spectrum for the generated free radicals.

In relation to the different irradiation protocols, G1 showed the strongest EPR spectrum signal at T0 and for the CT, with a value of 100%±6%, with all other samples being compared with this result. The concentration of free radicals for G2 at the CT was equivalent to 53%±6% from G1 and 87% ± 6% from G3. Regarding the samples from the middle and apical thirds for all groups, the variation in the intensity of the EPR spectrum was not significant, indicating that the radiation did not influence the free radical formation in the depth correspondent to G1 and G3. Comparatively to G1, the EPR spectrum intensity reduction was 47%±6% for CT in G2 and 13%±6% in G3 (Table 6.4).

Table 6.3 Experimental groups and material evaluated

Group	Sample		Treatment	Factor to be assessed
G1	Three translucent fiberglass posts White Post DC (FGM), number 1	Three sections of the cervical third	Irradiated (40 s)	FR concentration of the cement AllCem (FGM) 10 min (T0) and 24 h (T1) after the cement mixture
		Three sections of the middle third		
		Three sections of the apical third		
G2	Three translucent fiberglass posts White Post DC (FGM), number 1	Three sections of the cervical third	Not irradiated	
		Three sections of the middle third		
		Three sections of the apical third		
G3	Three translucent fiberglass posts White Post DC (FGM), number 1	Three sections of the cervical third	Irradiated (40 s) with the cementing line sealed	
		Three sections of the middle third		
		Three sections of the apical third		

Table 6.4 Relative concentration of free radicals in the samples 10 min after mixing base paste and catalyst

	Sample		
Group	CT	MT	AT
G1	100 ± 6%	No varies	No varies
G2	53 ± 6%	No varies	No varies
G3	87 ± 6%	No varies	No varies

The decrease observed in the relative concentration of free radicals for CT in G2 (Table 6.4) was significant when compared to G1 and G3, because the cement polymerization in G2 was exclusively chemical. When compared to G1, the observed decrease for CT in G3 might have occurred due to the use of a barrier at the post-silicon interface, which limited the passage of the curing light to only through the post.

Comparing G1 and G3 for CT, the light emitted may have been absorbed and transmitted by the cement located at the post-silicon interface, indicating that sealing the cementing line can diminish the initial amount of generated free radicals affecting the conversion degree of monomers to polymer.

It is possible to notice that the translucence and light conduction capability of the post is significant only in the first 8 mm of restoration, once the irradiation protocol did not interfere in the amount of generated free radicals for MT and AT.

6.4.1.2 Depth of Cure of the Translucent Fiberglass Post

The influence that chemical and physical polymerization exerts on the conversion degree of the resin cement can also be observed when evaluating the free radical concentration for samples obtained from the cervical, middle, and apical sections in G1, G2, and G3 and individually at T0 and T1 (Figs. 6.19 and 6.20).

At T0 (Fig. 6.19), the free radical concentration decreased for MT (12–14 mm) and AT (18–20 mm) in relation to CT (6–8 mm) in G1 and G3. In G1, the initial free radical relative concentration is greater than in G3 because the radiation emitted by the curing light is transmitted by the post and the post-silicon interface. This fact contributes to the facilitation of the polymerization of the resin cement; consequently, a faster conversion degree in G1 was observed (Fig. 6.19), considering that the reaction was already started and a portion of the generated free radicals in G1 was already reacted at the time of observation. In turn, G2 did not show decreasing for CT, MT, and AT, because the cement polymerization in all sections was exclusively chemical.

When analyzing points where the light incidence is relevant 10 min after mixing base paste and catalyst (CT, Table 6.4), it is possible to notice that the light can duplicate the concentration of free radicals at these points. Analyzing Fig. 6.19 it is possible to see that the concentration of free radicals decreased about 50% from CT to AT, for G1 and G3, such that it is possible to conclude that the light does not reach the deepest points of the restoration.

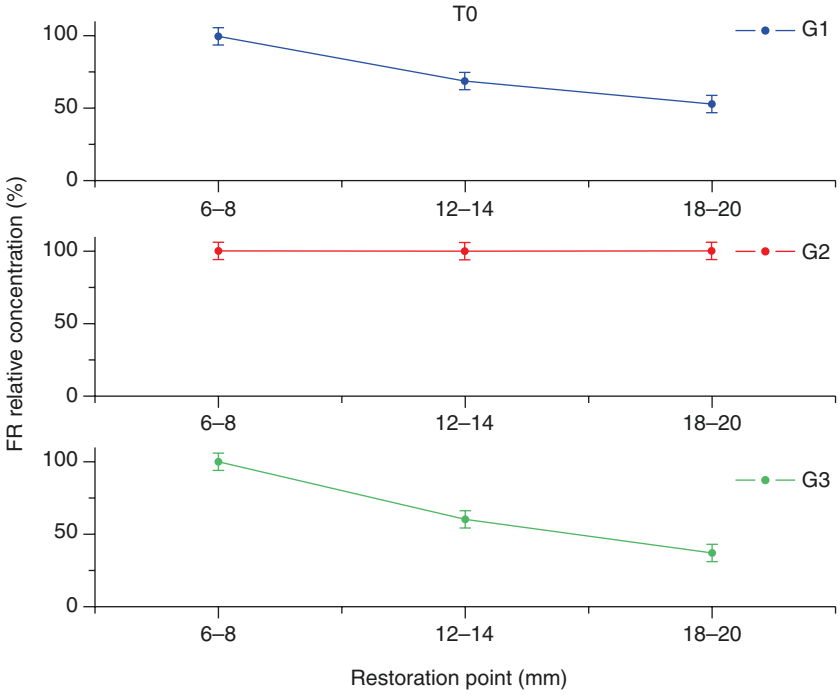

Fig. 6.19 Relative concentration of FR in T0

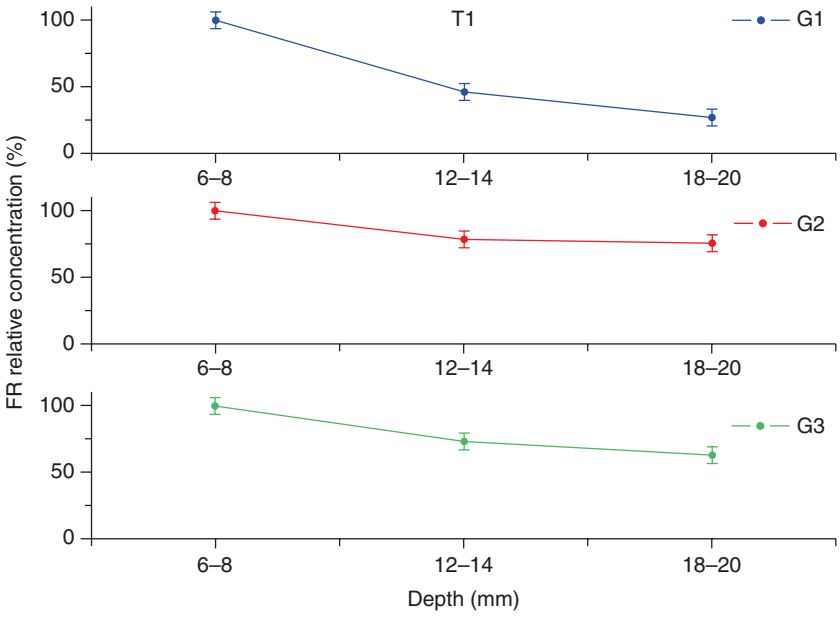

Fig. 6.20 Relative concentration of FR in T1

Twenty four hours after cementation (Fig. 6.20), G1 showed greater decrease in relative concentration of free radicals with depth compared to G3, opposite behavior shown in Fig. 6.19. It occurs because in T0 greater amount of free radicals are generated in G1 than that in G3, which affects the conversion degree. The greater the amount of free radicals generated, the greater is the conversion degree. The decay rate of concentration of initiators depends on the initial concentration of initiators.

The irradiation time, radiation power, and distance from the curing device to the irradiated region directly influence the conversion degree and, consequently, the mechanical properties of a cement and in the bond strength of the fiberglass post to the radicular dentin. Other variables that can influence the amount of generated free radicals and the conversion degree are the post diameter, arrangement of the fibers, composition, translucence degree, and the cementation line thickness. In the present experiment, the power and time were kept constant, 1500 mW/cm^2 and 40 s, respectively, as well as the distance from the curing device to the cemented post. However, based on the present results, a reduction of the luminous intensity with increasing depth of a simulated root canal was observed.

6.4.2 Influence of Geometrical Configuration of the Post on the Depth of Cure

This experiment aimed to evaluate the relative concentration of FRs in samples from the dual-cure resin cement AllCem (FGM, Joinville, SC, Brazil) of shade A1 by electron paramagnetic resonance (EPR) at different restoration points after cementation of a prefabricated translucent fiberglass post White Post DC no. 1 in a simulated root canal (Table 6.5). The post was sectioned to obtain cylindrical and conical samples in order to study the influence of the geometrical configuration of

Table 6.5 Experimental groups and material evaluated

Group		Sample	Curing protocol	Factor assessed
G1	Three cylindrical translucent fiberglass posts, White Post DC (FGM), no. 1 (ClP-1)	Three sections of the cervical quarter	Cement light cured for 40 s	Relative concentration of FR of the cement AllCem (FGM) at two moments in time: T10 min after mixing the cement and T24 h after
		Three sections of the middle quarter		
		Three sections of the deep quarter		
		Three sections of the apical quarter		
G2	Three conical translucent fiberglass posts, White Post DC (FGM), no. 1 (CnP-1)	Three sections of the cervical quarter	Cement light cured for 40 s	
		Three sections of the middle quarter		
		Three sections of the deep quarter		
		Three sections of the apical quarter		

the translucent fiberglass post in the generation of free radicals, which are known to be responsible for the polymerization of the resin cement. Here cervical means the post part closest to the light source and apical the farthest part [5].

After post cementation, the resin cement was photopolymerized for 40 s using a light-emitting diode (LED) (Radii Plus – SDI®, São Paulo, SP) with a potency of 1500 mW/cm^2 and in contact with the exposed ClP-1 and CnP-1. Ten minutes after mixing the resin cement, the set ClP-1/CnP-1 and the AllCem cement was removed from the silicone. With a double-sided fine-grained diamond disc (Microdont, Socorro, SP, Brazil) at low speed, the portion of the posts that remained outside following cementation were sectioned, leaving 8 mm corresponding to the cemented part. This part was sectioned every 2 mm to obtain the samples, cervical quarter (CQ, post portion closest to the polymerization device), middle quarter (MQ), deep quarter (DQ), and apical quarter (AQ), with the samples from ClP-1 allocated to group 1 (G1) and samples from Cn-1 allocated to group 2 (G2) (Fig. 6.20). All samples were obtained in the same conditions of light, temperature, and oxygen.

Figure 6.22a shows EPR spectrum of the dual-cured resin cement due to the superposition of radical I and radical III, and Fig. 6.21b shows the superposition of EPR spectra with MgO:Mn^{2+} standard for cervical, medium, deep, and apical quarters of the conical configuration and illustrates how the comparison can be done. The first line in the EPR spectrum (Fig. 6.22b) is the superposition of the third line of the MgO:Mn^{2+} standard with the first line of the resin cement free radical, and the last line in the spectrum is the superposition of the fourth line of the standard with the last line of the free radical. The EPR signal amplitude of free radicals for all groups was normalized with the line intensity of the third line of the MgO:Mn^{2+} standard to compare variances in the intensity of the free radical signal (central line). As cervical quarter showed the most intense EPR signal amplitude and thus the greatest concentration of free radicals, it was taken as the reference point to study the variation on the relative concentration of free radicals between the samples into the group, so that the data presentation is relative to cervical quarter in each group (taken as 100%).

The EPR spectra in X-band (~9 GHz) were obtained in a JEOL (JES-PE-3X) spectrometer at room temperature, and the microwave power (1 mW), modulation

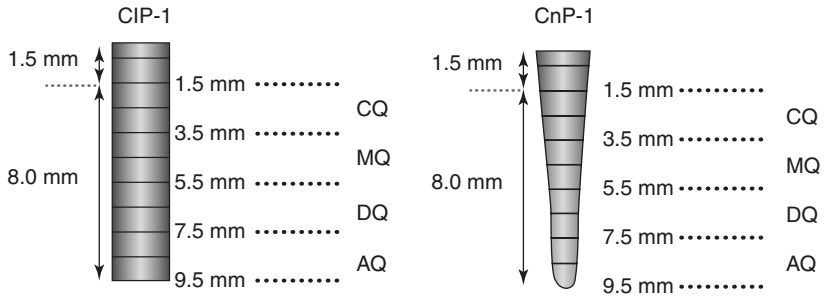

Fig. 6.21 Schematic representation of samples from ClP-1 (G1) and CnP-1 (G2)

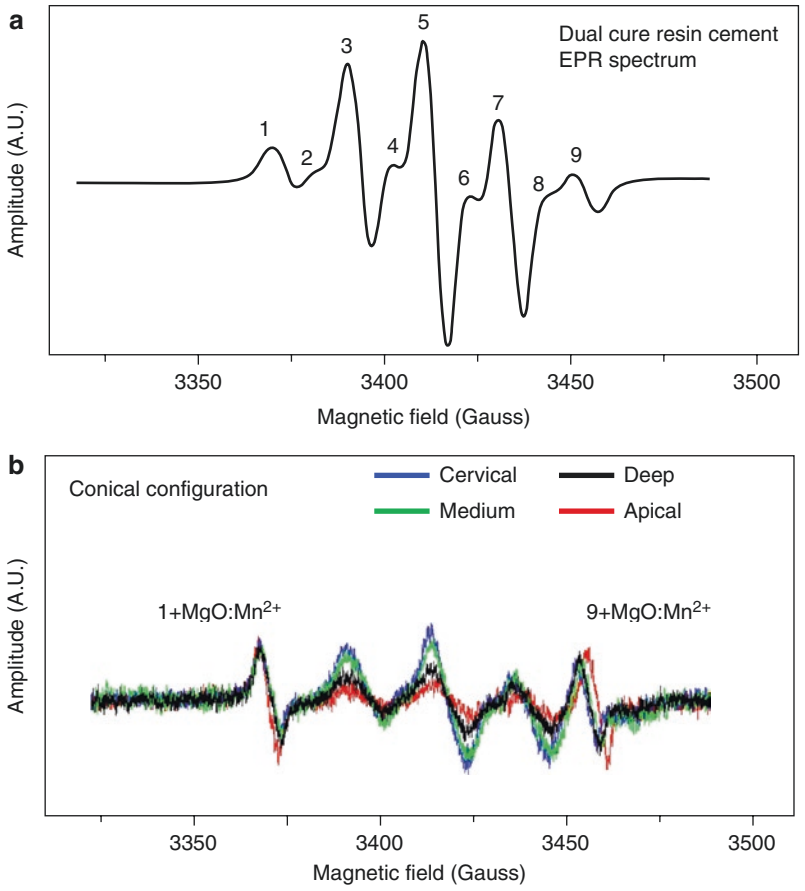

Fig. 6.22 (**a**) Nine-line EPR spectrum of the dual-cured resin cement, characteristic of methacrylate radicals. (**b**) Superposition of EPR spectra obtained from the CQ, MQ, PQ, and AQ of conical configuration at T10 min

amplitude (0.40 mT), and modulation frequency (100 kHz) were set to avoid signal saturation and were maintained constant. A JEOL standard sample MgO:Mn^{2+} was used as an intensity standard and g marker. The 2 mm samples were inserted into the EPR tube (3 mm inner diameter) and investigated immediately after 40 s of irradiation. As the EPR signal intensity is proportional to the amount of paramagnetic species in the sample and this quantity is directly related to the light incidence in the sample, it is possible to use the MgO:Mn2+ as the intensity standard and evaluate differences in the FR concentration for different sections of the post. Each sample was analyzed 10 min (T10 min) and 24 h (T24 h) after mixing the cement. The samples were always carefully handled with tweezers stored in aluminum packets to ensure no influence could be attributed to external light and prevent external contamination.

The best signal to noise ratio among the three replicate EPR spectra obtained for each sample in each experimental group was used for data treatment due to accordance between replicates (Fig. 6.22).

In Fig. 6.22, the first line is the third line of the MgO:Mn^{2+} standard superimposed on the first FR line, and the last line is the fourth resonance line of the standard superimposed on the ninth FR line. The nine lines in the EPR spectrum are typical of methacrylate radicals. The EPR signal intensity for all groups was normalized with the MgO:Mn^{2+} third line intensity. In addition, the EPR signal intensity of the samples in G2 was normalized with respect to the amount of the cement mass, since the resin cement volume is not the same for all samples in this group; because the fiberglass post is conical, a reduction in diameter occurs in the cervical to apical direction. This type of normalization is not required in G1.

For data treatment, it was assumed that the relative FR concentration of the cervical sample (CQ) for G1 and G2 was 100%, because these samples are the first surface and showed the most intense EPR signal and thus the greatest relative FR concentration. The FR concentration for all the other samples in the group was obtained relative to the CQ (Tables 6.6 and 6.7).

Different decay rates were observed in the relative concentrations of FR when comparing the two geometrical configurations (Table 6.6). The G1 MQ showed no variation in the relative concentration of FR with respect to the CQ at T10 min. This indicates that no significant decrease in the light transmission through the cylindrical post occurred that affected the FR concentration at depths up to 5.5 mm. In the DQ, the FR concentration was 84% and in the AQ 70%, clearly indicating that the effectiveness of the light transmission through the post decayed, such that the FR concentration decreased 16% at 6–8 mm in depth and 30% at 8–10 mm. This difference can be explained by the increase in the distance of the DQ and AQ in relation to the radiation source, even when using 1.500 mW/cm^2 of power. In G2, a decrease in the FR concentration was verified for all samples compared with the CQ; the MQ, DQ, and AQ decreased 11, 41, and 72% in relative FR concentration, respectively. The distance between the LED device and the samples analyzed was a significant factor influencing the decay in FR concentration in both G1 and G2. However, for

Table 6.6 Relative FR concentration at T10 min

Group	CQ (1.5–3.5 mm)	MQ (3.5–5.5 mm)	DQ (5.5–7.5 mm)	AQ (7.5–9.5 mm)
G1	100% ± 6%	100% ± 6%	84% ± 6%	70% ± 6%
G2	100% ± 6%	89% ± 6%	59% ± 6%	28% ± 6%

Table 6.7 Relative FR concentration at T24 h

Group	CQ (1.5–3.5 mm)	MQ (3.5–5.5 mm)	DQ (5.5–7.5 mm)	AQ (7.5–9.5 mm)
G1	100% ± 6%	94% ± 6%	98% ± 6%	91% ± 6%
G2	100% ± 6%	83% ± 6%	40% ± 6%	14% ± 6%

This table presents the relative FR concentrations of the samples analyzed 24 h (T24 h) after mixing the base paste and catalyst

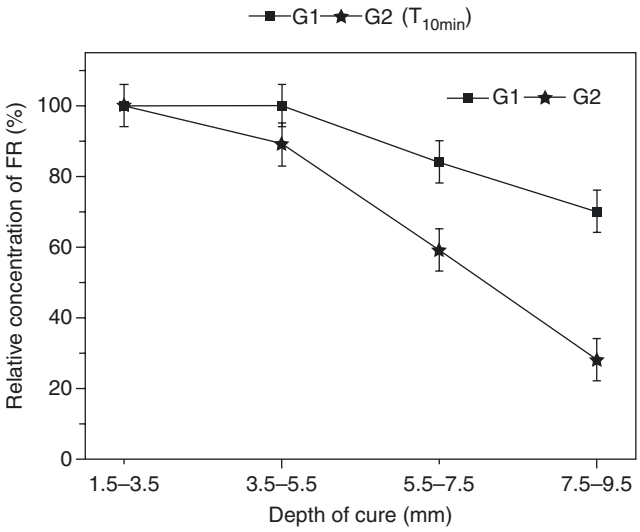

Fig. 6.23 Comparison of the decrease in the relative concentration of free radicals for G1 and G2 in T10 min

G2, the geometrical configuration also influenced light transmission through the post, and thus the relative amount of FR observed in the samples tested was lower (Fig. 6.23).

In our research, it is evident that the shape of the translucent fiberglass post influenced the transmission capacity of the light emitted from the LED device and thus the FR concentration in the dual-cured resin cement, both at T10 min and T24 h.

The diameter of ClP-1 was constant throughout the post length, as well as the amount of epoxy resin and fiberglass. However, in CnP-1, the diameter ranges from 1.6 to 1.25 mm from the cervical to the apical extremities. Considering the variation in FR concentration between G1 and G2 samples, the importance of the diameter of the post in light transmission was confirmed.

In his research, the results showed that the larger the post diameter, the better the results of polymerization of the composite resin at greater canal depth. Regarding the actual effectiveness of transmission of the light emitted by the LED device and its influence on the degree of conversion of FR in resin cement throughout the length of the cemented post, Shadman et al. observed that a translucent quartz fiber post permitted a greater degree of conversion in dual-cured resin cement compared with an opaque post. The authors suggested that this result could be related to the difference in refractive index between glass fiber and epoxy resin in the post. When the light passes through the fiber, it crosses the resin-fiber interface at a higher angle of incidence, which allows reflection to other fibers, resulting in an increase in total light transmittance.

The behavior of light rays emitted by the LED device through interfaces with different refractive indexes could explain the results observed in G1 (Table 6.7), where the DQ showed a higher relative FR concentration compared with the MQ.

A portion of the radiation may have been transmitted through the fiberglass and epoxy resin, while another part may have been absorbed by the mass of the resin cement. The light may also have been directly transmitted by cement located at the post-matrix interface. However, this occurs at low intensity, since the greater part of the light undergoes scattering and absorption when passing from the external environment to the cement mass. Due to changes in the geometrical configuration of CnP-1, the effectiveness of light transmission from the post to the cement is reduced because of the difference in refractive indices.

In relation to the post configuration for ClP-1, at T10 min, no difference was observed between the CQ and MQ. When analyzed at T24 h, the relative FR concentration in the MQ decreased 11% compared with the CQ.

Table 6.7 presents the relative FR concentrations for samples analyzed 24 h (T24 h) after mixing the base paste and catalyst. Compared with the CQ, G1 showed conformity between the relative FR concentrations, such that the MQ, DQ, and AQ showed 94, 98, and 91%, respectively. A larger decrease in the relative FR concentrations was observed for G2 as the depth increased. In this group, the relative FR concentrations were 83, 40, and 14% for the MQ, PQ, and AQ, respectively. During irradiation, the concentration of FR rapidly increases up to a maximum value, depending on the concentration of initiators, depth of cure, and other factors. When irradiation is terminated, the concentration of FR decreases exponentially to zero due to the consumption of FRs when converting monomers to polymers. At depths where the maximum amount of generated FRs is considerably smaller, the EPR spectra obtained 24 h after irradiation shows a relative concentration of FR that is lower than in those samples with a significantly greater concentration of FR.

References

1. Vicentin BLS, Netto AM, Dall'Antonia LH, Di Mauro E, Blümich B. Real-time polymerization monitoring in a dual-cured resin cement by magnetic resonance. Polym Bull. 2017; https://doi.org/10.1007/s00289-017-2007-1.
2. da Silva Fontes A, Vicentin BLS, Valezi DF, da Costa MF, Sano W, Di Mauro E. A Multifrequency (X-, Q-, and W-band) EPR and DFT study of a photopolymerizable dental resin. Appl Magn Reson. 2014;45(7):681–92.
3. Vicentin BLS, Netto AM, Blümich B, Di Mauro E. Identification of free radicals generated by different curing modes in a dental resin cement. Appl Magn Reson. 2016;47(9):1003–14.
4. Vicentin BLS, Salomão FM, Hoeppner MG, Di Mauro E. Influence of geometrical configuration of a translucent fiberglass post on the polymerization of a dual cure resin cement analyzed by epr spectroscopy. Appl Magn Reson. 2016;47(2):211–22.
5. Salomão FM, Vicentin BLS, Contreras EFR, Hoeppner MG, Di Mauro E. The influence of a translucent fiberglass post on the polymerization of dual cure resin cement analyzed by electron paramagnetic resonance. Materi Res. 2015;18(5):1023–8.
6. Truffier-Boutry D, Gallez XA, Demoustier-Champagne S, Devaux J, Mestdagh M, Champagne B, Leloup G. Identification of free radicals trapped in solid methacrylated resins. J Polym Sci A Polym Chem. 2003;41(11):1691–9.